Basic Optical Sensor Model

THOMAS WINZELL

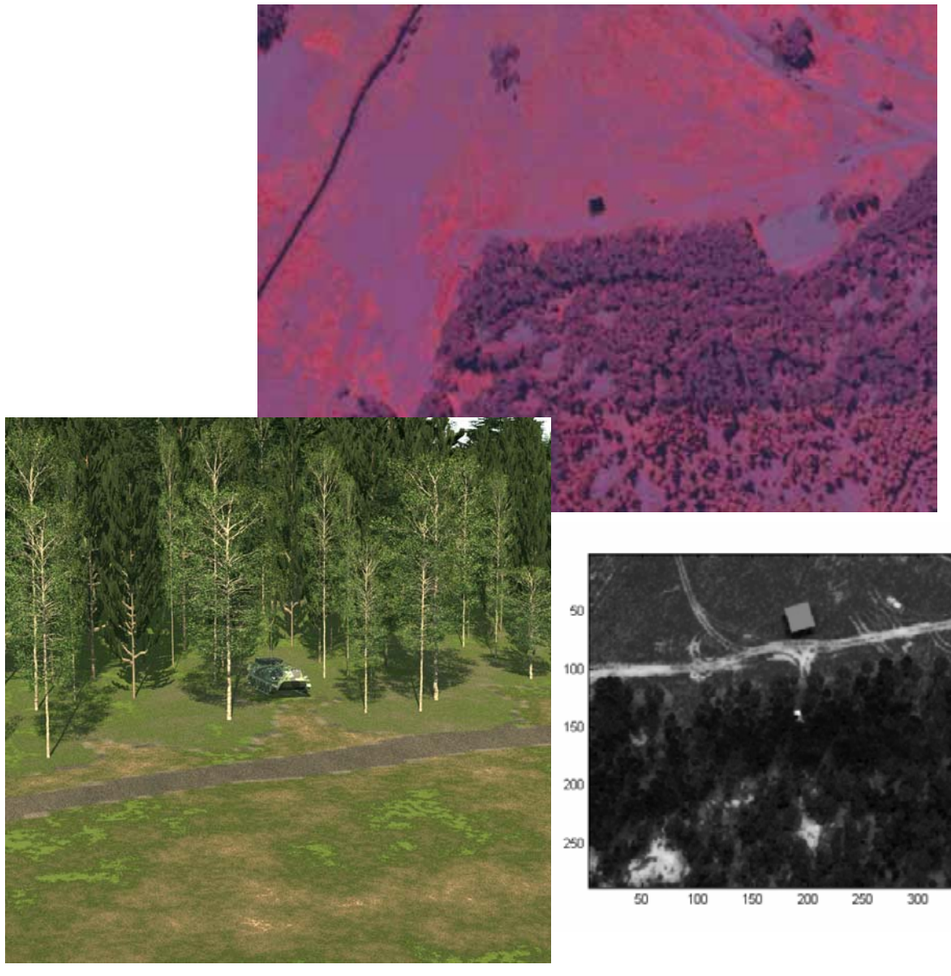

FOI, Swedish Defence Research Agency, is a mainly assignment-funded agency under the Ministry of Defence. The core activities are research, method and technology development, as well as studies conducted in the interests of Swedish defence and the safety and security of society. The organisation employs approximately 1250 personnel of whom about 900 are scientists. This makes FOI Sweden's largest research institute. FOI gives its customers access to leading-edge expertise in a large number of fields such as security policy studies, defence and security related analyses, the assessment of various types of threat, systems for control and management of crises, protection against and management of hazardous substances, IT security and the potential offered by new sensors.

FOI
Defence Research Agency
Sensor Technology
P.O. Box 1165
SE-581 11 Linköping

Phone: +46 13 37 80 00
Fax: +46 13 37 81 00

www.foi.se

FOI-R--2135--SE Scientific report
ISSN 1650-1942 November 2006

Sensor Technology

Thomas Winzell

Basic Optical Sensor Model

FOI-R--2135--SE Scientific report Sensor Technology
ISSN 1650-1942 November 2006

Issuing organization	Report number, ISRN	Report type
FOI – Swedish Defence Research Agency Sensor Technology P.O. Box 1165 SE-581 11 Linköping	FOI-R--2135--SE	Scientific report
	Research area code 4. C4ISTAR	
	Month year November 2006	**Project no.** E3082
	Sub area code 42 Above water Surveillance, Target acquistion and Reconnaissance	
	Sub area code 2	

Author/s (editor/s)	Project manager
Thomas Winzell	Jörgen Ahlberg
	Approved by
	Sponsoring agency Swedish Armed Forces
	Scientifically and technically responsible Ingmar Renhorn

Report title
Basic Optical Sensor Model

Abstract

In this work, a sensor model has been outlined mainly as an addition to synthetic imagery generation tools such as CAMEO-SIM and McCavity. The sensor model is based on defining and identifying physical parameters and models for describing optics, detector matrix, noise, motion and atmospherics among other imaging specifics. A short review of MTF is given as well as a noise model for semiconductor pixel based sensors, especially CCD focal plane arrays. A discussion of FOI specific experimental sensor systems is given as well as some critical parameters for model implementation of these systems. Two sensor modelling examples are described as well as some selected results.

Keywords

Sensor model,MTF, synethic imagery,noise,CAMEO-SIM,McCavitySensor model, MTF, synthetic imagery, noise, CAMEO-SIM, McCavity

Further bibliographic information	Language English

ISSN 1650-1942	Pages 38 p.
	Price acc. to pricelist

Utgivare FOI - Totalförsvarets forskningsinstitut Sensorteknik Box 1165 581 11 Linköping	**Rapportnummer, ISRN** FOI-R--2135--SE	**Klassificering** Vetenskaplig rapport
	Forskningsområde 4. Ledning, informationsteknik och sensorer	
	Månad, år November 2006	**Projektnummer** E3082
	Delområde 42 Spaningssensorer	
	Delområde 2	
Författare/redaktör Thomas Winzell	**Projektledare** Jörgen Ahlberg	
	Godkänd av	
	Uppdragsgivare/kundbeteckning FM	
	Tekniskt och/eller vetenskapligt ansvarig Ingmar Renhorn	

Rapportens titel

Grundläggande optisk sensormodell

Sammanfattning

I detta arbete beskrivs sensormodelling, främst för att komplettera existerande datorverktyg för syntetisk bildgenerering. Sensormodellen baseras på definierade och identiferade fysikaliska parameterar för att bland annat beskriva optik, detektormatris, brus, rörelse, och vissa atmosfäriska egenskaper. En kort översikt för MTF ges liksom en modell för beskrivning av sensorbrus för halvledarbaserade sensorer, speciellt för CCD fokalplansarrayer. Några av FOIs experimentella sensorsystem beskrivs liksom kritiska parametrar för att implementera dessa system. Två exempel på sensormodell beskrivs tillsammans med utvalda resultat.

Nyckelord

Sensormodell, MTF, syntetiska bilder, brus, CAMEO-SIM

Övriga bibliografiska uppgifter	**Språk** Engelska
ISSN 1650-1942	**Antal sidor:** 38 s.
Distribution enligt missiv	**Pris: Enligt prislista**

1. Introduction

FOI is quite well equipped with synthetic scene and target generation codes for hyper spectral optical signature prediction, such as CAMEO-SIM [1], RadThermIR [2], and McCavity [3]. Furthermore, FOI also has several experimental sensor systems, both prototype and commercially available sensors, from the visual wavelength domain, through the near infrared and out into the mid- and long wave infrared. Relevant and realistic sensor models are not only needed for direct sensor development issues, but also for prediction of optical signatures for, e.g. camouflage assessment and techniques, detection range estimations, and detection algorithm training and testing. In this work, a sensor system model has therefore been developed to be applied primarily to synthetic imagery, but could also in principle be used to real imagery for, e.g. simple image reconstructions.

There are of course several ways in how a sensor system model can be designed. One way is to start from first principle physics; another way could be to only implement sensor system critical parameters such as field-of-view (fov), pixel resolution and waveband, and hence creating a very crude sensor model. In this work, the sensor model is more of the latter approach by identifying critical parameters that set building blocks of a sensor system. These building blocks are, among others, relationships for modelling the optics, noise considerations, detector and electronic parameters etc. Furthermore, all the different models for the different parts of the sensor system should be implemented in such a way that the model could approach, at least in theory, a first principle physics one.

The second section will deal with theoretical aspects of the sensor model, the third will deal with the implementation of such a model and the two finishing parts will deal with implementation and applied examples of the model.

2. Theoretical remarks

A model for a sensor system can be defined and divided into different parts, and include different aspects of a sensor system. In this work, the sensor is divided in two parts, the optics and the detector. Each of these parts can be said to have critical parameters, which without a sensor cannot exist. In figure 2.1, the fate of a photon (or rather the fate of a differential radiance image) travelling through the model is outlined. The input is of either a synthetic radiance image from

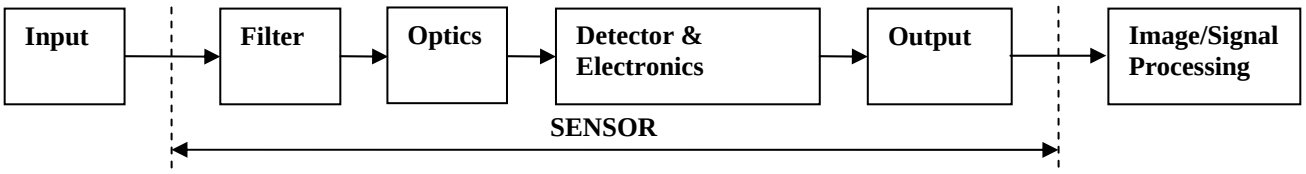

Figure 2.1. Simple sketch of the sensor model

software or experimental data, e.g. from an imager or simply from a radiometer. Any atmospheric consideration that is not included in the synthetic imagery tool should be applied before any sensor modelling, i.e. it should be already included in the 'input' box in figure 2.1. The radiation goes first through any spectral selective filter, secondly through the optics, and then it is converted to an electric signal in the sensor. The output produced can be either a radiometric unit such as radiance or apparent temperature, or just a digital number image reflecting the dynamics of the sensor. Each box in the sensor definition in figure 2.1, can be subdivided into one or several critical or non-critical parameters. For instance, the filter is nothing else than a spectral transmission curve, the optics have several parameters such f-number, optical transmission etc, and so does the detector/electronics box in figure 2.1, defining instantaneous field-of-view (IFOV), fill factor, conversion gain etc. The first subsection will shortly deal with output from synthetic software. The second subsection will discuss the different parameters that the boxes in figure 2.1 imply, what they mean and their necessecity in a sensor system model.

2.1 Optical signature codes

As previously mentioned, FOI has a number of very competent commercial optical signature codes [1-3].

- CAMEO-SIM [1] is a 32 bit hyper spectral synthetic imagery generator from 0.3 μm to 14 μm for simulating targets in backgrounds. By feeding CAMEO-SIM with information on 3D terrain and 3D object geometry, spectral reflectance and thermal material properties, and with spectral and thermal weather data (through MODTRAN [4]) synthetic optical imagery can be obtained via a spectral response, a pixel resolution and a fov.

- RadThermIR [2] is a 2.5 dimensional (not complete 3D mesh) thermal solver for targets such as military vehicles, and delivers a time dependent thermal solution for the object with information on object material properties, weather and limited surrounding information. There is an important link between CAMEO-SIM and RadThermIR that allows for complete object-on-background and background-on-object interactions to take place. The reason is to make use of RadThermIR's competent thermal solver and only use the limited 1-dimensional thermal layer solver in CAMEO-SIM for periphery optical signature calculations [1,2].

- McCavity [3] delivers hyper spectral optical signatures in IR for airframes including inlet and outlet with plume radiation. The information needed in McCavity is a flow field

solution of both airframe and jetplume together with a spectral atmosphere, the spectral waveband, fov and pixel resolution. Both CAMEO-SIM and McCavity delivers output in the form of (spectral) radiance among other formats. Figure 2.2 shows a CAMEO-SIM [1] generated RGB image and corresponding thermal infrared image of a well-modelled part of the Kvarn military field outside Linköping. In figure 2.3, an IR image simulation of a simple UAV frame with corresponding jet engine plume simulated using McCavity [3] is shown.

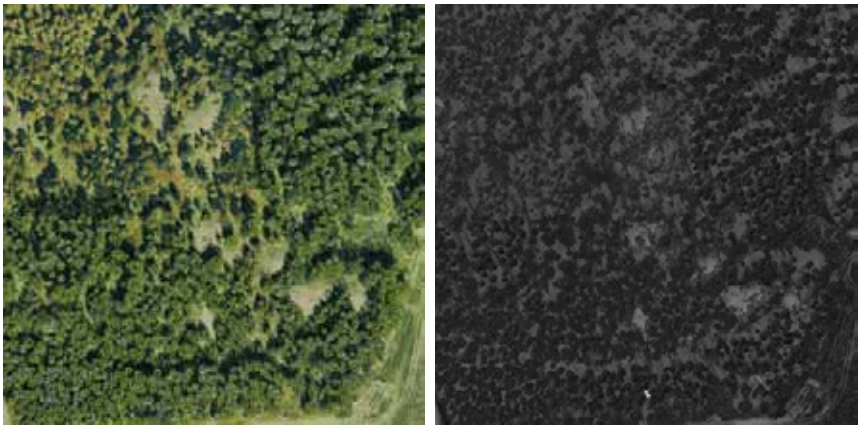

Figure 2.2. Simulated RGB (left) and corresponding longwave-IR (right) image from an airborne sensor using the synthetic image generation tool CAMEO-SIM.

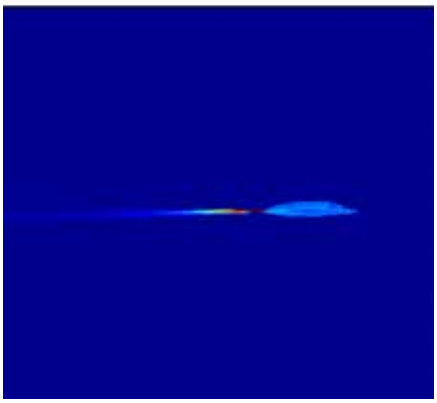

Figure 2.3. Simulated IR radiance image of UAV frame with jet engine plume.

These quite competent synthetic imagery generation tools lack more sophisticated means of sensor modelling. Both McCavity and CAMEO-SIM can only define spectral waveband response, fov, and the sensor pixel resolution. Missing are such effects such as optical blur, detector blur, motion blur, noise, and some atmospheric effects such as turbulence. In this work, basic requirements and formulations are outlined for constructing such a sensor system model.

2.2 Sensor system properties

In this work, the sensor has been divided into an optics part and a detector part. Both these parts can be naturally divided into parameterised subparts such as f-number, and optical transmission for the optics and spectral response, sensor resolution, and electronic noise for the detector. In this section the identified parts of the sensor system will be divided all the way down to physical parameters that a user can alter for a specific existing sensor system.

2.2.1 Optical properties

There are several physical phenomena that come into play when radiation travels through an optical system. The lens system has an effective f-number which together with the radiation wavelength gives the optical blur spot [5,6]. The diffraction limited blur has a diameter given by [5,6]

$$d_{diffraction} = 2.44\lambda(F/\#)_{img-space}, \tag{2.1}$$

where λ is the wavelength, and *F/#* is the f-number in image space. The f-number in image space is given by the image distance divided by the aperture dimension when the object is not at infinity, while when the object is at infinity the f-number becomes instead the focal length divided by the aperture dimension. Throughout this work, objects are considered to be at infinity so for the rest of this document, the f-number is defined as

$$F/\# = \frac{f}{D}, \tag{2.2}$$

where *f* is the focal length (or the effective focal length of the whole lens system), and *D* is the aperture dimension (usually a diameter). Furthermore, most optical systems are designed using many individual lenses and mirrors, where each has different refractive index and shape. For modelling purposes, the optical system is treated as one element with an *effective* focal length.

The impulse response, *h(x,y)*, of an optical system determines the smallest detail that the system is capable of forming [5,6,7]. The impulse response in optical systems is usually called the point spread function (PSF) [7]. The PSF describes the spatial illumination in the image plane when a point source is applied. Image radiance distribution, *g(x,y)*, is the ideal image radiance distribution, *f(x,y)*, convolved with the impulse response, *h(x,y)*, i.e.

$$g(x,y) = f(x,y) * h(x,y). \tag{2.3}$$

The convolution theorem states [7,8] that convolution in spatial domain is product in frequency domain, i.e. taking the Fourier transform, $\Im$, of both sides of equation 2.3 yields:

$$\Im\{g(x,y)\} = \Im\{f(x,y) * h(x,y)\} \Leftrightarrow G(u,v) = F(u,v) \times H(u,v), \tag{2.4}$$

where *F(u,v)* is the object spectrum, *H(u,v)* is the spectrum of the impulse response or rather the *transfer function*, and *G(u,v)* is the spectrum of the image. The most important result of equation (2.4) is that the transfer function, *H(u,v)*, relates object and image spectra multiplicatively. This means that analysing a combination of subsystems can be done multiplicatively using transfer functions rather than convoluting the corresponding impulse responses. For an optical system, the normalised *H(u,v)* is known as the *optical transfer function* (OTF), which is a complex function in general. (A complex OTF means that the PSF is not symmetric in general.) The OTF therefore has both a magnitude and a phase portion. The magnitude of the OTF is called the *modular transfer function* (MTF), and the phase portion is referred to as the *phase transfer function* (PTF). In summary:

$$OTF \equiv \Im\{h(x,y)\} = |H(u,v)|e^{j\phi(u,v)}, \tag{2.5}$$

$$MTF \equiv |H(u,v)|, \tag{2.6}$$

and

$$PTF \equiv \phi(u,v)\,. \tag{2.7}$$

From an optical system point of view it can be seen that the MTF describes decrease in magnitude, hence contrast, and is therefore the most important transfer function of equations (2.5)-(2.7). It is also seen through the convolution theorem that independent MTFs could be cascaded, i.e. [5,8]:

$$MTF_{Total} = \prod_i MTF_i\,. \tag{2.8}$$

The MTF can be defined as *the ratio of the image modulation to the object modulation at all spatial frequencies*. The contrast or modulation is further defined by [5]:

$$Modulation \equiv \frac{I_{Max} - I_{Min}}{I_{Max} + I_{Min}} = \frac{ac}{dc}\,, \tag{2.9}$$

where I_{Max} and I_{Min} is the maximum and minimum of the signal at the image plane, respectively. Inspecting equation (2.9) it can be seen that modulation corresponds to the amount a function varies about its mean value, divided by that mean value. Another way of looking at equation (2.9) is to view it as how readily the fluctuations will be discernible against a dc background. For an image system this means that the input signal is "smeared out" around its mean value resulting in decreased contrast. In figure 2.2, a sinusoidal input is degraded through an MTF resulting in a smeared sine wave with reduced contrast.

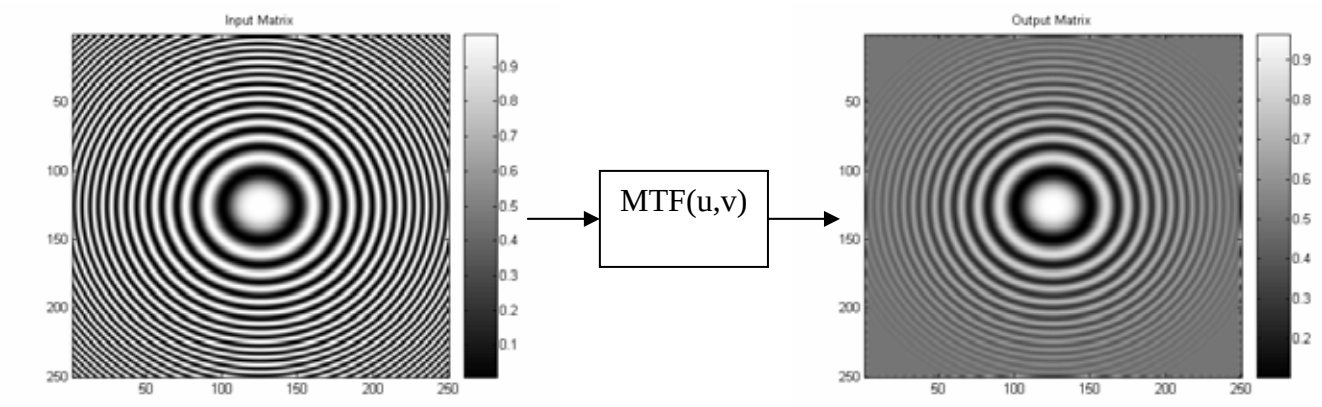

Figure 2.2. Example of degrading a sinusoidal input using an MTF.

2.2.1.1 Optical MTF

The aperture of most optical systems has a circular geometry with refracting telescopes. Furthermore, the optical system consists of several lenses with varying focal lengths and varying indices of refraction. Often one lens offsets the aberration of another, which implies that linear system theory cannot be employed to describe the individual elements. This means that the lens system must be considered as a whole, which in relation to modeling applications results in that the optical system is treated as a single lens with the same effective focal length and aberrations as the total lens system. Diffraction limited MTFs can be expressed exactly, while MTFs for aberrations and defocusing are treated as approximations. Optical spatial frequencies are 2-dimensional with the frequency ranging from -∞ to +∞, while the highest spatial frequency that can be reproduced by the optical system is limited by the optical cutoff frequency. This is especially important for synthetic imagery as sampling usually has already been carried out.

Diffraction limited MTF for a circular aperture can be expressed as [9]

$$MTF_{Diffraction} = \frac{2}{\pi}\left[\cos^{-1}\left(\frac{\rho}{\rho_{oco}}\right) - \frac{\rho}{\rho_{oco}}\sqrt{1-\left(\frac{\rho}{\rho_{oco}}\right)^2}\right], \tag{2.10}$$

when $\rho < \rho_{oco}$, and 0 elsewhere. The optical cutoff frequency is given by

$$\rho_{oco} = \frac{D_0}{\lambda}, \tag{2.11}$$

where D_0 is the aperture diameter, and λ is the wavelength.

Aberrations in an optical system can be approximated in many ways. One empirical relationship is given by Shannon [10], which governs most aberrations of real lens systems:

$$MTF_{Aberrations} \approx 1-\left(\frac{W_{rms}}{A}\right)^2\left[1-4\left(\frac{\rho}{\rho_{oco}}-\frac{1}{2}\right)^2\right], \tag{2.12}$$

when $\rho < \rho_{oco}$. In equation (2.12) W_{rms} is the root-mean-square (rms) wave-front error expressed as a fraction of waves, and $A = 0.18$. Marceal [11] suggests that the rms wave-front error is related to the peak-to-peak wave front error by $W_{rms} = \frac{W_{pp}}{3.5}$. $W_{pp} = 0.25$ simulates the wave-front error that typically occurs during manufacturing. The approximation in equation (2.12) is valid for small wave-front errors ($W_{pp} < 0.5$), which is a reasonable limit for well-designed optics [12].

Fixed focus systems can be quite out of focus if the target of interest is outside the depth of field [13]. Such defocus can be described by the approximation (good up to 2.2 waves) suggested by Shannon [14]:

$$MTF_{Defocus} = \frac{2J_1\left(8\pi\frac{\rho}{\rho_{oco}}\left[1-\frac{\rho}{\rho_{oco}}\right]\right)}{8\pi\frac{\rho}{\rho_{oco}}\left(1-\frac{\rho}{\rho_{oco}}\right)}, \tag{2.13}$$

where $J_1()$ is the first order Bessel function. If the defocus errors are less than 0.5 wave peaks, only the first four terms in the Bessel function are needed to give a good approximation, i.e.

$$J_1(x) = \frac{x}{2} - \frac{x^3}{16} + \frac{x^5}{384} - \frac{x^7}{18432}. \tag{2.14}$$

Equations (2.10) through (2.14) gives a good basis for optical image degradation.

2.2.1.2 Central obscuration – Cassegrainian telescope

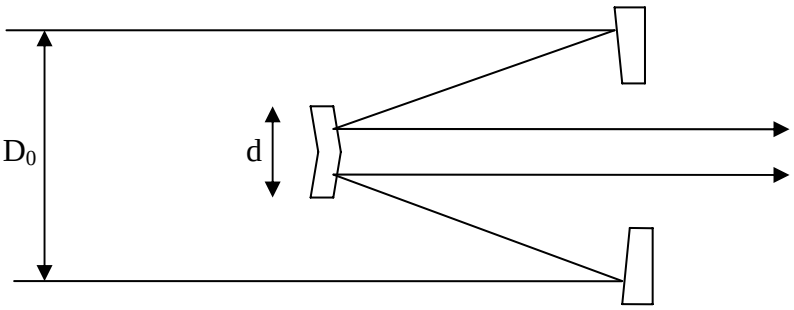

Figure 2.3. Cassegrainian telescope with aperture diameter D_0 and obscuring diameter d. First mirror tends to be a paraboloid, second a hyperboloid. [15].

Figure 2.3 shows a Cassegrainian telescope with a central obscuration. The diffraction limited MTF for an optical system with a central obscuration is given by [15]

$$MTF_{Diffraction} = \frac{A + B + C}{1 - R^2}, \tag{2.15}$$

where

$$A = \frac{2}{\pi}\left[\cos^{-1}(X) - X\sqrt{1 - X^2}\right], \text{ when } 0 < X < 1, \tag{2.16}$$
$$A = 0, \text{ elsewhere.}$$

$$B = \frac{2R^2}{\pi}\left[\cos^{-1}(Y) - Y\sqrt{1 - Y^2}\right], \text{ when } 0 < Y < 1, \tag{2.17}$$
$$B = 0, \text{ elsewhere.}$$

$$C = -2R^2, \text{ when } 0 < X < \frac{1 - R^2}{2}, \tag{2.18}$$
$$C = \frac{2R^2}{\pi}\sin\alpha + \left(\frac{1 + R^2}{\pi}\right)\alpha - \frac{2\left(1 - R^2\right)}{\pi}\tan^{-1}\left[\left(\frac{1 + R}{1 - R}\right)\tan\left(\frac{\alpha}{2}\right)\right] - 2R^2,$$
$$\text{when } \frac{1 - R}{2} \le X \le \frac{1 + R}{2},$$
$$C = 0, \text{ when } X > \frac{1 + R}{2}.$$

$R = \frac{d}{D_0}$, where d is the obscuration diameter, and D_0 is the aperture diameter as shown in figure 2.3, $X = \frac{f_x}{f_{oco}}$, where f_x is the spatial frequency, and f_{oco} is the optical cutoff frequency, $Y = \frac{X}{R}$, and finally $\alpha = \cos^{-1}\left(\frac{1 + R^2 - 4X^2}{2R}\right)$. Note that when $d = 0$, equation (2.15) goes to equation (2.10).

2.2.1.3 Angular dependent sampling

In some cases, the optical system has an angular dependence, i.e. the signal smearing can be different when comparing light passing along the optical axis and light coming from other parts of the lens. This is usually an increasing effect when the system's field-of-view increases. As this is from a sampling perspective a position dependent effect, MTFs cannot be applied as is. Such considerations have to be done in the image domain. An approximate method when considering synthetic imagery (or image reconstruction) might be to calculate the MTFs belonging to the different PSFs in the image domain that characterizes the optical angular dependence. A set of new synthetic images are calculated using these calculated MTFs. The new image is then constructed by using this set of new images, i.e. identifying in the image where a certain MTF is no longer valid (from the PSF positions), and then replace image pixels belonging to the wanted PSF. In this way the rest of the image degrading processes such as motion, detector blur etc can be applied using cascaded MTFs.

2.2.2 Sensor properties

The sensor in an optical image system contains a number of different bits and pieces. In this work only photon detectors are considered even if thermal detectors also are of importance [16]. When the radiation has passed through the lens system it is focused onto an array of semiconductor rectangles, i.e. pixels. Each semiconductor material has its physical cutoff wavelength given by the relationship [17]

$$\lambda_{cutoff} = \frac{hc}{\varepsilon_{gap}} \ , \tag{2.19}$$

where ε_{gap} is the energy bandgap of the semiconductor, h is Planck's constant, and c is the speed of light. Any radiation of wavelength, $\lambda > \lambda_{cutoff}$, will not result in an electron being lifted into the conduction band for this specific semiconductor material. E.g., normal silicon (that you find in your digital cameras) has a bandgap $\varepsilon_{gap} \approx 1.12$ eV at 300 K, which according to equation (2.19) indicates that detectors made out of Si can not absorb photons of wavelengths longer than about 1.1 μm. It can be seen from equation (2.19) that the smaller the bandgap, the longer the wavelength cutoff as for InSb with a bandgap of about 0.22 eV giving a cutoff wavelength of about 5.6 μm.

When optical power falls onto the photosensitive region of the semiconductor detector, the absorption of a photon generates an electron-hole pair. The electron in the conduction band and the hole in the valence band move in opposite directions under the influence of an applied field leading to a photocurrent. The photocurrent, i, is the response of the incident absorbed photon. In general, this photocurrent is directly proportional to the incident power, P, i.e.

$$i = RP \tag{2.20}$$

where the proportionality constant is called the responsivity of the detector and is given by

$$R = \frac{\eta q}{h\nu}, \tag{2.21}$$

where q is the electron charge, h is Planck's constant, ν is the optical frequency, and where η is the quantum efficiency of the photodetector. This important characteristic of the detector material, the quantum efficiency η, i.e. the (average) number of electrons excited to the conduction band per incident photon. This quantity is normally wavelength dependent, i.e $\eta = \eta(\lambda)$. E.g., for standard

IR detector materials such as HgCdTe (often called MCT) the quantum efficiency is about 0.5 for quite a broad waveband (from about 2 μm into the thermal long wave infrared) [18] by altering the stoichiometry of the HgCdTe material. For Si (often applied in consumer CCD applications) on the other hand the quantum efficiency has a more complicated dependency on wavelength [18].

Examples of semiconductor materials for imagers are Si used in UV and visble imager applications, InSb and HgCdTe for midwave-IR (MWIR) and longwave-IR (LWIR), and extrinsic-Si materials for very long wavelengths [18]. Another important detector is the quantum well infrared photodetector (QWIP), often made using AlGaAs/GaAs with GaAs as substrate as a material system combination [19]. The QWIP is most often used for 8-9 μm applications, but by taylormaking the quantum well layers other wavelengths can be reached [19].

Spectral responsivity is also an important characteristic of a photon sensor. Ideally, photon detectors have linear proportionality with wavelength, i.e.

$$R(\lambda) = \frac{\lambda}{\lambda_{cutoff}} R(\lambda_{cutoff}) \text{ when } \lambda \le \lambda_{cutoff}, \text{ and } R(\lambda) = 0 \text{ when } \lambda > \lambda_{cutoff}. \quad (2.22)$$

Equation (2.22) simply states that for a photon detector it requires a higher photon flux to make a Watt at longer wavelengths. The spectral flux on a detector with a spectral responsivity *R(λ)* [V/W] gives therefore an output (in V) as

$$U = \int_0^\infty \phi_{\lambda,\det}(\lambda) R(\lambda) d\lambda = \int_0^\infty L_\lambda A\Omega R(\lambda) d\lambda, \quad (2.23)$$

where $\phi_{\lambda,\det}(\lambda) = \frac{2c^2 h}{\lambda^5 \left(e^{\frac{hc}{kT\lambda}} - 1 \right)} A\Omega = L_\lambda A\Omega$ is the photon flux [W/m] for a detector area *A* subtending a solid angle Ω with *h* as Planck's constant, *c* the speed of light, *k* Boltzmann's constant, *T* is the source temperature, and λ as the wavelength. Equation (2.23) states that the detector output is a function of those wavelengths where the spectral radiance and spectral responsivity both are non-zero.

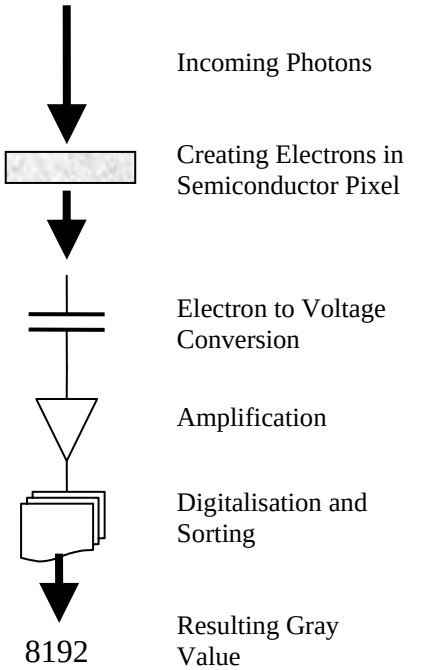

Figure 2.3. Photons to digital number.

The size of a detector array is a function of first of all the number of pixels in the horizontal and vertical directions. The detector element size and the distance between the detector elements, i.e. pitch, completes the detector array size. For a fixed optical system, i.e. a fixed f-number, it can be seen through equation (2.1) that the blur spot increases with wavelength. Therefore, there is no need to make smaller pixels than those defined through equation (2.1) with respect to the wavelength of interest.

An important property of the detector array is also the so called fill factor. A fill factor of 100% means that the detector size is equal to the detector pitch. The detector pitch is defined as the distance from adjacent pixel centers. Normally, the fill factor is less than 100%. E.g. for the FOI MWIR optical system MultimIR [20] the fill factor is about 83%.

In figure 2.3 a simple sketch showing the fate of how incident photons are converted into a gray value in a semiconductor sensor system. Incoming photons are converted to electrons at the pixel during integration time. The electrons are converted to a voltage, then amplified, digitised and sorted into a gray value. When constructing the sensor model the first number of interest is then how many photons correspond to a certain digital number, or rather the so called conversion number, *K*, e.g. the digital number (DN) per radiance, *L*. The inverse of *K* then means the radiance required to raise the digital number by one. This conversion number can be dealt with in a sensor model in a number of ways. It can be measured, i.e. the total sensor system can be calibrated (not necessarily a linear conversion and with a zero offset) and this measurement is used to go from realistically modelled radiance values to the specific sensor's gray value or it can be calculated or rather estimated. For a sensor system working in the thermal IR domain this can be done by letting the total conversion gain give e.g. half the dynamic range of the sensor for the radiance in the waveband at hand at e.g. a source temperature of 300 K reaching the detector. In the visible domain the analogy would be letting the 6000 K hot sun light scatter on materials (earth) with reflections values within a certain range, e.g. 10% to 90% of reflection.

The next number of interest to add to the signal is of course noise. Noise is present for all sensor systems and is definitely a critical parameter for any optical sensor system. There are of course many different sources of noise, all the way from fundamental noise such as photon and electron noise to amplifier and quantisation noise [21]. One starting point is by dividing the main noise contributors into temporal and spatial noise. The temporal noise describes the variation in a single pixel observed over time, while spatial noise describes the variation that occur from pixel to pixel when all pixels are irradiated with the same amount of radiative intensity and the temporal noise is averaged out. Temporal noise harbors such noise sources as photon/electron noise, dark current, and amplifier noise. Spatial noise includes two main components, offset noise and gain noise. The former is often also referred to as fixed pattern noise (FPN) while the latter is often noted as photo-response non-uniformity (PRNU) [21]. A noise model based on first principle physics is of course quite difficult. Therefore, as a basic noise model, e.g. an implementation of Gaussian white noise is quite handy to have. Let e.g. the mean of such a Gaussian noise function be zero and the variance an (experimentally) estimated percentage of the dynamic range for the optical sensor system at hand.

2.2.2.1 Noise model

In the previous section, important noise properties of a semiconductor sensor system were discussed. In so called charge-coupled devices (CCDs), photons are caught in a potential well in each pixel. When the integration or the exposure has passed, the electrons are sequentially shifted out of the sensor. Each charge packet is loaded into a capacitor yielding a voltage proportional to the number of electrons in the package, and hence proportional to the number of photons collected. Following the sensor noise model outlined by [21], it is suitable to start by noting that the total number of photons, n_q, arriving during exposure time is Poisson distributed i.e.

$$n_q \approx P(\mu_p), \tag{2.24}$$

where the variance equals its mean by

$$\sigma_p^2 = \mu_p . \tag{2.25}$$

By estimating the collected light, the noise level of the light can be estimated given by the signal-to-noise ratio, i.e. square root of the mean itself

$$SNR_p = \frac{\mu_p}{\sigma_p} = \sqrt{\mu_p}, \tag{2.26}$$

and more light gives typically a better image. Each photon has a probability, η, to create a free electron, which means that the number of electrons are also Poisson distributed, i.e. with a mean

$$\mu_e = \eta\mu_p\,, \tag{2.27}$$

and with a variance given by

$$\sigma_e^2 = \eta\mu_p = \eta\sigma_p^2\,, \tag{2.28}$$

where η is the total quantum efficiency as discussed in the previous section. When the pixel saturates no more free electrons are created even if more photons are arriving. This means that equations (2.27) and (2.28) converts to $\mu_e \to \mu_{e,sat}$, and $\sigma_e^2 \to 0$.

The number of (mean) electrons generated for a certain (integrated) radiance, *L*, for one pixel is given by (for white light refer to equations (2.51) through (2.53).

$$\mu_e = \frac{L\tau A_{Pixel}\eta\Omega}{\left(\frac{hc}{\lambda}\right)}, \tag{2.29}$$

where τ is the integration time, A_{Pixel} is the area of a pixel, η is the quantum efficieny, *h* is Planck's constant, *c* is the speed of light, λ is the wavelength, and Ω is the solid angle given by

$$\Omega = \frac{A}{R^2} = \frac{A_{Pixel}}{F_l^2}\,, \tag{2.30}$$

where *A* is the area in object space, *R* is the distance to the target, and F_l is the effective optical focal length.

The total conversion from electrons to digital gray values can be modelled by the linear scaling factor, *K* as introduced in section 2.2.2. *K* gives the digital number per electron [DN/e^-], or inversely the number of electrons required to increase the digital output with one unit. Included in the total conversion factor is usually a gain, *G*, for gain user control (as well as brightness control), i.e. [21]

$$K = K_0 G\,. \tag{2.31}$$

Dark noise and any offset added to the signal inside the sensor can be modelled via Gaussian white noise [21] where the number of noise electrons is given by

$$n_d \approx N\left(\mu_d, \sigma_d^2\right), \tag{2.32}$$

with a variance σ_d^2 and a mean μ_d. By combining equations (2.24)-(2.32) the mean output signal is given by

$$\mu_y = K\left(\mu_e + \mu_d\right) = K\left(\eta\mu_p + \mu_d\right), \tag{2.33}$$

and with a variance given by

$$\sigma_y^2 = K^2\left(\sigma_e^2 + \sigma_d^2\right) = K^2\left(\eta\mu_p + \sigma_d^2\right). \tag{2.34}$$

A good quality measure of an image is the signal-to-noise ratio (SNR) of the digital output signal. The SNR in digital output can be defined as [ref]:

$$SNR_y = \frac{\mu_y - \mu_{y,dark}}{\sigma_y} = \frac{\eta\mu_p}{\sqrt{\left(\eta\mu_p + \sigma_d^2\right)}}, \tag{2.35}$$

with

$$\mu_{y,dark} = K\mu_d \tag{2.36}$$

being the signal of the sensor without (external) input flux. For a visual camera this signal comes from the so called dark current (no external flux), but for a thermal camera the signal is a sum of dark current electronics as well as thermal photons coming from various camera parts. In fact, this bias can be quite large and can in these cases be a substantial part of the sensor's dynamic range. By plotting the mean digital number for different input (e.g. a thermal plate sitting at different temperatures) for a fixed exposure time the total "dark" signal is the offset in such a plot. The offset in a plot of the mean digital number for a thermal plate at a fixed temperature against the exposure time then gives the dark current.

Another important quality measure of a digital sensor is the so called dynamic range (DYN) defined as the ratio between the largest and smallest detectable signal levels, i.e.

$$DYN = \frac{\mu_{p,\max}}{\mu_{p,\min}} = \frac{\mu_{y,\max}}{\sigma_{y,temp,dark}}. \tag{2.37}$$

The term spatial noise was previously introduced, i.e. the variations that occur from pixel to pixel when all pixels are illuminated with the same light intensity (and the temporal noise is averaged out) [21]. Spatial noise includes two components, offset noise and gain noise. This means that equation (2.34) for describing the noise in each pixel must be extended to include spatial noise as well, i.e.

$$\sigma_{y,total}^2 = \sigma_{y,temp}^2 + \sigma_{y,spatial}^2 = K^2\left[\overbrace{\eta\mu_p + \sigma_d^2}^{temporal} + \overbrace{\sigma_o^2 + S_g^2\eta^2\mu_p^2}^{spatial}\right], \tag{2.38}$$

where σ_0^2 is a constant part modelling the inter-pixel variation of the spatial noise offset (FPN), and a last term in equation (2.38) which models the variation of the gain (PRNU). By identifying that

$$\begin{aligned}\sigma_{y,spatial}^2 &= K^2\left[\sigma_0^2 + S_g^2\eta^2\mu_p^2\right] = \sigma_{y,spatial,dark}^2 + K^2S_g^2\eta^2\mu_p^2 = \\ &= \sigma_{y,spatial,dark}^2 + S_g^2\left(\mu_y - \mu_{y,dark}\right)^2\end{aligned} \tag{2.39}$$

the gain noise can be written as

$$S_g = \frac{\sqrt{\sigma_{y,spatial}^2 - \sigma_{y,spatial,dark}^2}}{\mu_y - \mu_{y,dark}}. \tag{2.40}$$

The offset noise σ_0 is then given by (setting $\mu_p = 0$ in equation (2.39))

$$\sigma_0 = \frac{\sigma_{y,spatial,dark}}{K}. \tag{2.41}$$

Equation (2.38) introduces a new SNR measure given by

$$SNR_y = \frac{\eta\mu_p}{\sqrt{\left(\eta\mu_p + \left(\sigma_d^2 + \sigma_0^2\right) + S_g^2\eta^2\mu_p^2\right)}}. \tag{2.42}$$

The mean output (gray value or digital number) is given by

$$\mu_y = \frac{1}{N}\sum_{j=1}^{N} y_j, \tag{2.43}$$

where y_j is the output for pixel j, and where N is the number of pixels.

The temporal noise can be estimated using the equation (which is a little bit different from the equation suggested by Dierks [21] where only two images were used for temporal noise estimation which might be enough)

$$\sigma_{y,temp,i}^2 = \sum_{j=1}^{M}\frac{\left(y_{ij} - \langle y_i\rangle\right)^2}{M-1}, \tag{2.44}$$

where i denotes the pixel, M is the number of images used, y_{ij} is the output (digital number) for pixel i and image j, and $\langle y_i\rangle$ is the average output for pixel i. By taking the mean of multiple images until the temporal noise is averged out and then calculate the total noise of the average image gives a good estimation of the spatial noise (if enough images are used) [21]. The spatial noise is then given by

$$\sigma_{y,spatial}^2 = \sum_{j}\frac{\left(y_j - \langle y\rangle\right)^2}{N-1}, \tag{2.45}$$

where y_j is the output for pixel j from the mean of a number (enough) of images, $\langle y\rangle$ is the mean digital output in the averaged image, and where N is the number of pixels for the CCD sensor. When it comes to the spatial noise of a thermal sensor this cannot be given by equation (2.39). The reason is the often seen strong correlation between the variation of bias and gain for each pixel's response as well as the spatial correlation from pixel to pixel. This is due to such different effects as pixel variations (semiconductor thickness, stoichiometry, area, aspect ratio, etc), narcissus patterns and overall varying operating conditions giving rise to fixed pattern noise. In the work by Renhorn [22], the nonuniformity of a sensor is modelled starting from the nonuniformity deviation and assuming proportionality between mean grey value and the gain slope variation, i.e.

$$\Delta Y_{i,j} = \Delta Y_{i,j}^{bias} + \Delta G_{i,j}\mu_y, \tag{2.46}$$

where

$$\Delta Y_{i,j} = Y_{i,j} - \mu_y, \tag{2.47}$$

with $Y_{i,j}$ being the digital number for pixel i,j, μ_y is given by equation (2.43), and $\Delta G_{i,j}$ is the gain variation for pixel i,j. The bias variation and the gain variation, often called correction coefficients, are obtained from a two point correction scheme at two different signal levels. For further information on nonuniformity measurements refer to section 4.1. The two coefficients in equation (2.46) are highly correlated and can be described by a multivariate normal density function [22]. The nonuniformity variance in equation (2.39) can then be altered to the more correct expression

$$\sigma_{y,spatial}^2 = \sigma_{spatial,bias}^2 + K^2\eta^2\mu_p^2\sigma_{gain}^2 + 2K\eta\mu_p\sigma_{spatial,bias}\sigma_{gain}\,. \tag{2.48}$$

A corresponding signal-to-noise ratio, SNR also follows [22].

From the photon transfer method [21] the conversion gain of the system is given by

$$K = \frac{\sigma_{y,temp}^2 - \sigma_{y,temp,dark}^2}{\mu_y - \mu_{y,dark}}\,. \tag{2.49}$$

The quantum efficiency of the system can be estimated computing

$$\eta = \frac{\mu_y - \mu_{y,dark}}{K\mu_p}\,. \tag{2.50}$$

Expanding this noise model from monochromatic light to white light, the number of collected photons whose wavelength is inside the interval $[\lambda, \lambda + d\lambda]$ can be expressed as

$$d\mu_p = \frac{A_{Pixel}L(\lambda)R(\lambda)\tau\Omega}{hc}\lambda d\lambda\,, \tag{2.51}$$

where A_{Pixel} is the pixel area, τ is the integration time, L is the radiance at the optics, R is any spectral selection done (e.g. transmission filters), h is Planck's constant, Ω is the solid angle (see equation (2.32)), and c is the speed of light. Using equation (2.28) the differential number of generated electrons is then given by

$$d\mu_e = \frac{A_{Pixel}\tau L(\lambda)\Omega}{hc}\lambda\eta(\lambda)d\lambda\,, \tag{2.52}$$

where $\eta(\lambda)$ is the effective spectral quantum effieciency. Integration over the wavelength interval $[\lambda_{\min}, \lambda_{\max}]$ then gives

$$\mu_e = \int_0^{\mu_e} d\mu_e = \frac{A_{Pixel}\tau\Omega}{hc}\int_{\lambda_{\min}}^{\lambda_{\max}} \lambda\eta(\lambda)L(\lambda)d\lambda\,. \tag{2.53}$$

2.2.2.2 Detector MTF

It was mentioned above that the detector fill factor often was less than 100%. This means that all radiation passing through the optical system telescope will not contribute to the sensor output, i.e. some of the radiation will fall inbetween pixels. Furthermore, the radiation sensitive area is often smaller than the geometrical size of the pixel (affecting also the effective quantum efficieny), which also reduces signal output. From a synthetic scene generating perspective, this is quite difficult to handle. One way is to sample synthetic radiance in a very high resolution matrix and then summing together signal in contributors corresponding to the sensor pixels and throwing

away signal falling in between. Another way is to use averaging MTF for smearing the signal in the pixels and hence reducing contrast to more realistically levels. By using the MTF from a scanning rectangular element, but with an upper frequency limit determined by the Nyquist criteria, a 2-dimensional Sinc function can be obtained [5,23,24,25]:

$$MTF_{Detector} = \frac{\sin(\pi f_x w_x)\sin(\pi f_y w_y)}{\pi f_x w_x \pi f_y w_y}, \tag{2.54}$$

for $|f_i| \le \frac{1}{2w}$ (and 0 elsewhere), and where f_x and f_y are the spatial frequencies in [m^{-1}] on the detector, and w_x and w_y are the dimensions of the rectangular detector element in [m]. Equation (2.54) assumes full coverage of the detector (i.e. a fill factor of 100%), which most likely is not true. A way of getting a more accurate (but still averaging) description is to use the detector element pitch. In this case, equation (2.54) (in frequency units of [rad^{-1}]) converts to

$$MTF_{Detector} = \frac{\sin\left(\pi f_x \frac{p_x}{F_l}\right)\sin\left(\pi f_y \frac{p_y}{F_l}\right)}{\frac{\pi f_x p_x}{F_l} \times \frac{\pi f_y p_y}{F_l}}, \tag{2.55}$$

for $|f_i| \le \frac{1}{2p_i}$ (and 0 elsewhere) with a pitch, p_i, and focal length F_l.

2.2.3 Motion

Another important process reducing image quality is motion. There are two main motion processes degrading imagery for staring optical systems, linear motion and random motion. If v is the relative velocity between the sensor and the scene, and D, is the distance between the scene and the sensor, then the sensor has moved the angular distance

$$a_l = \frac{v t_{Integration}}{D}, \tag{2.56}$$

radians during the integration time, $t_{Integration}$, of the sensor system. The MTF then due to linear motion can be expressed as [26]

$$MTF_{Linear} = \frac{\sin(\pi a_l f_x)}{\pi a_l f_x}, \tag{2.57}$$

where f_x is the spatial frequency, and a_l is the angular movement. Expanding equation (2.57) to 2 dimensions gives [24]

$$MTF_{Linear} = \frac{\sin(\pi a_x^l f_x + \pi a_y^l f_y)}{\pi a_x^l f_x + \pi a_y^l f_y}, \tag{2.58}$$

where a_i^l, $i = x, y$ is the angular movement in the x- and y-direction, respectively. Included in the expression of the angular movement of equation (2.58) is the integration time of the detector. The precise value that should be used for the integration time depends on the system. For a staring image collecting system the integration time can be expressed as [24]

$$t_{Integration} = \frac{1}{F_R I_F}, \tag{2.59}$$

where F_R is the frame rate and, I_F is the interlace factor for the detector [24]. When the image is observed by a human observer the eye blends many frames of data. The exact integration time of the eye is not without controversy, but according to the FLIR92 documentation [27] a value of 0.1 s is recommended as the integration time of the human eye.

Vibration or jitter result in high frequency random motion, which can be described by a Gaussian MTF given by [28]

$$MTF_{Random} = e^{-2\pi^2 \sigma_r^2 \rho^2}, \tag{2.60}$$

where σ_r is the root-mean-square random displacement in units of rad [29]. Equation (2.60) is only valid if the image has moved enough during the integration time, so that the central limit theorem holds. The parameter, σ_r, is usually unknown, but typically if it is less than 10% of the detector angular subtense (DAS), α = (detector size / effective focal length), the sensor system image quality is not significantly affected.

2.2.4 Atmospheric considerations

The atmosphere affects the radiance of a scene of interest in many ways. It contributes by e.g. sky shine and scattered sun light, it reduces scene signal by spectral transmission, and blur the signal due to random fluctuations in the atmospheric refractive index caused by random changes in air pressure and temperature (so called turbulence). In many synthetic optical scene generating codes, such as CAMEO-SIM [1], highly qualified atmospheric prediction codes are included such as MODTRAN [4]. This means that many atmospheric effects are included and can be modelled from first principle physics in programs such as MODTRAN [4].

When it comes to radiation scattering in the atmosphere, the radiation scattering phenomenon can be divided into three components. Firstly, radiation originating from the scene that is scattered out of the line-of-sight (LOS) contributes to the extinction. Radiation originating from outside the scene scattered into the LOS contributes to the path radiance, and thirdly radiation originating from within the scene scattered into the LOS will blur the image. This third affect, i.e. the blurring can mathematically be considered as an MTF.

2.2.4.1 Turbulence

As previously mentioned, turbulence originates from random fluctuations in the atmospheric refractive index caused by random changes in air pressure and temperature. Even if these fluctuations are small they do cause the radiation to arrive at different angles at the receiver resulting in image motion, distortion and blurring [30]. Turbulence is most dramatic within a few meters of ground level and it affects image quality more dramatic when the turbulence is close to the optical sensor system.

Modelling turbulence from first principles is a very difficult task, but for many practical considerations the so called refractive index structure parameter, C_n^2 [31,32,33], is enough for practical optical turbulence predictions. C_n^2 is a measure of the magnitude of the turbulence and has a very strong diurnal dependence. There are many factors that influence C_n^2, e.g. strong solar

heating, very dry ground, surface roughness, limited wind are all factors that increases C_n^2, heavy overcast daytime sky, high winds, and wet surfaces together with high humidity decreases C_n^2.

Turbulence is a dynamic phenomenon, i.e. it will affect image features differently at each instant of time. Practically, this means that turbulence MTF on any image will deviate significantly from the average. Furthermore, turbulence effects are not spatially symmetrical distributed and imagery will change constantly. Therefore, any MTF assigned to turbulence will represent an average as MTF theory only applies to stationary processes. A simple turbulence MTF will be given, taken from the work by Holst [30], but should be treated as a simple form to illustrate and estimate the magnitude of the effect. In many cases, the MTF created by turbulence can be approximated by

$$MTF_{Turbulence} \approx e^{-3.44\left(\frac{1000\lambda f_x}{r_0}\right)^{\frac{5}{3}}}, \tag{2.61}$$

where r_0 becomes

$$r_0 = 0.185\lambda^{\frac{6}{5}}\left[\sec(\theta)\int_0^{\frac{R}{\sec(\theta)}}\left(\frac{h\sec(\theta)}{R}\right)^{\frac{5}{3}} C_n^2(h)dh\right]^{-\frac{3}{5}} \tag{2.62}$$

for viewing a target at the elevation angle θ. $\sec(\theta) = \frac{1}{\sin(\theta)}$, R is the slant path measured from the target (i.e. the target is at $R = 0$), h is the altitude, λ is the wavelength, and

$$C_n^2(h) = C_{n0}^2 h^{-\frac{4}{3}}, \tag{2.63}$$

where C_{n0}^2 is the refractive index structure parameter at one meter altitude [34]. A rule-of-thumb is that if $\frac{D_0}{r_0} < 0.2$, where D_0 is the aperture diameter, then turbulence can be neglected.
Furthermore, for horizontal paths (where C_n^2 is considered to be a constant), r_0 becomes

$$r_0 = 0.185\left[\frac{8\lambda^2}{3RC_n^2}\right]^{\frac{3}{5}}, \tag{2.64}$$

where again R is the path measured from the target, λ is the wavelength, and C_n^2 is the refractive index structure parameter. Work has been done to model C_n^2 from registered weather parameters [35], where estimations of C_n^2 can be found. Typically, C_n^2 less than 10^{-15} $m^{-2/3}$ is considered as weak turbulence, moderate between 5×10^{-15} to 10^{-14} $m^{-2/3}$, and strong when C_n^2 is larger than 5×10^{-14}. These latter values together with equations (2.61)-(2.64) can be used to estimate average imagery degradation due to turbulence.

2.2.4.2 Aersol

When small angle scattering on aersols of radiation reaches the detector and have sufficient intensity to be detected, an image blur will be obtained. However, if the scattered radiation from the target is much lower than the scattered radiation from the background, the effect will be minor and can be neglected. The atmospheric transmittance will be replaced with the so called “classical” approximation when the scattered radiation intensity is significant. The transmittance is given by [4]

$$\tau_{Atmosphere}(\lambda) = e^{-\gamma(\lambda)R}, \tag{2.65}$$

where λ is the wavelength, R is the path length, and

$$\gamma(\lambda) = \sigma(\lambda) + k(\lambda), \tag{2.66}$$

is the spectral extinction coefficient divided into σ as the wavelength dependent scattering coefficient, and k being the absorption coefficient. The “classical” approximation is given by [36]

$$MTF_{Aerosol} = e^{-kR-\sigma R\left(\frac{f_x}{f_{aco}}\right)^2}, \tag{2.67}$$

when $f_x < f_{aco}$, and

$$MTF_{Aerosol} = e^{-kR-\sigma R}, \tag{2.68}$$

when $f_x \geq f_{aco}$. The aersol cutoff is given by

$$f_{aco} = \frac{a}{\lambda F_l}, \tag{2.69}$$

where a is the effective aersol radius in [m], and F_l is the focal length of the optical system. Inspecting equations (2.67) and (2.68), and comparing to equation (2.65) it can be seen that the aerosol MTF goes to the “normal” atmospheric transmission for spatial frequencies above the aersol cutoff given by equation (2.69). Please note that f_{aco} is very small for most optical systems. The extinction coefficient (equation (2.66)) can be obtained for most atmospheric conditions of interest from e.g. MODTRAN [4], and the effective aerosol radius has many dependencies such as regional, seasonal and weather [4], and can be obtain from many different sources such as direct experimental measurements [4,37].

2.2.5 Global and measured MTF

Throughout this section, several MTFs have been listed as averaging transfer functions for many important properties of a sensor and also atmosphere. An important characterisation of an optical sensor system is its total transfer function, i.e. the total system MTF, MTF_{System}, which could be said to be a cascade of many different MTFs describing the different parts of the system as indicated in equation (2.8). Even the atmospherics in the previous section can be included (due to the assumption of linearity) in such a cascaded MTF. There are several methods of measuring MTF [20], but usually these are done in one dimension, i.e. as a plot of modulation (response) versus spatial frequency or rather lines per unit length. Using the somewhat shaky assumption that the MTF is symmetric, a 2-dimensional MTF can be constructed by rotating the measured MTF

around zero spatial frequency. This can then be used as the global MTF of the sensor system in equation (2.4).

Another way of constructing a total sensor system MTF is by assuming a Gaussian function with a certain variance. For instance, the variance could be a certain percentage of the subtense angle of a pixel, i.e.

$$MTF_{Global} = e^{-2\pi^2 \sigma_{System}^2 f_x^2}, \tag{2.70}$$

where f_x is the spatial frequency, and σ_{System}^2 has the dimension of blur diameter, but will in fact be a system parameter with no real physical meaning. It could be made being a certain percentage (e.g. 100%) of detector size divided by focal length, i.e. the detector angular subtense (DAS). In this way, a global approximating MTF can be implemented and tested on how it influences image quality for the system as a whole.

3. Implementation

Implementing a sensor model can of course be carried out in a number of ways. There are mainly three fields interested in such a model illustrated by figure 3.1 below. Besides development of sensors, signature evaluation and algorithm development are fields where sensors and hence sensor models are of critical importance. Two discintions that can be made are also in the sensor model itself. Models can be developed (and used) from a total theoretical side (working with synthetic imagery), and from an experimental point of view, i.e. sensor characterisation and image

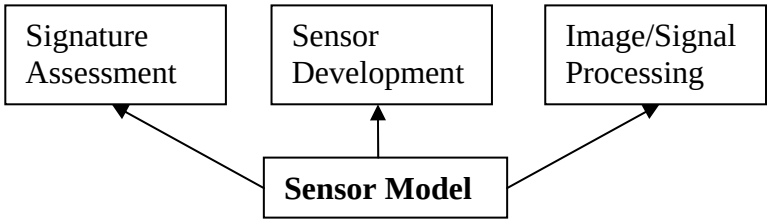

Figure 3.1. Sensor model fields of interest.

reconstruction and sensor calibration. As FOI have several optical sensor systems, there is an interest to have models for these systems as a basis. The systems are the Emerald, the MultimIR, and QWIP in the infrared [20, 37-40]. Added to these systems are a sensor system where all the important constituents can be chosen and parametrised to simulate more or less any sensor system (within reason). The first two sections will cover requirements on the sensor model from synthetic imagery generation, and sensor characterisation, respectivel. The next coming sections will each deal with one of the noted imagers, and finally a section with a sensor built from scratch.

3.1 Synthetic imagery

There are two main synthetic imagery codes at FOI that delivers hyperspectral output, CAMEO-SIM [1] and McCavity [3], where the former works from 0.3-14 μm, and the latter in the infrared region. Both codes set up observers in terms of hyperspectral wave band, fov, pixel resolution, and observer scene/target distance and view angle. Some atmospherics (defined and limited more or less by MODTRAN [4]) are included in both codes, while some atmospherics are not included (such as turbulence etc [30]). The two codes deliver output in several ways, but of interest for sensor modelling the main deliverable is spectral radiance for each defined pixel. There are a couple of ways of importing synthetic output to a sensor model. Complete pixel sampling to the pixel resolution of interest can be done within the synthetic scene generation code, or it can be done within the sensor model. This latter method means that a much higher pixel resolution is used when generating the spectral synthetic imagery, and then letting the sensor model down sample the imagery to the correct pixel resolution. It should be possible to use both these methods within the sensor model. The next issue is the question whether the correct spectral resolution and wave band selection should be done already when generating the synthetic imagery, or afterwards, inside the sensor model. In principle, hyperspectral synthetic imagery (limited by MODTRAN [4] in CAMEO-SIM [1], and by the band model in McCavity [3]) can be generated and then spectrally down sampled to the waveband and wavenumber of interest in the sensor model. A problem might be very large data sets which could cause inconvenience in data handling. Still, both methods should be available in the sensor model. As it at this stage exists no technique for remotely running synthetic scene generation programs such as CAMEO-SIM [1] and McCavity [3] from e.g. a Matlab sensor model, the requirements to be met of the sensor model can be summarised as follows. The sensor model should have the possibility to import:

i) hyperspectral imagery for user selected spectral downsampling,

ii) high pixel resolution to user selected downsampling,
iii) image sequences,
iv) radiance input in $Wm^{-2}sr^{-1}$.

It should be noted that besides the possibility of importing hyperspectral image sequences given in $Wm^{-2}sr^{-1}$, spectral selection/response bands (or wave band limits together with band resolution), fov, pixel resolution and perhaps sensor/target distance must also be imported into the sensor model. Some of these variables/functions should be default values for specific sensor models; some will be dependent on how the simulation at hand was carried out in the synthetic scene generation tool. Below is a list of variables/functions that has to exist for each and every synthetic image. These parameters have to be defined within the synthetic image simulation, i.e. outside any sensor model.

i) field-of-view in degrees,
ii) pixel resolution ,
iii) spectral band (or wave band limits with band resolution).

The sensor model will then either by user input or by specific sensor default values/functions process image(s) correctly. It should also be pointed out that any atmospheric effects that are not covered by the synthetic imagery generating tool (such as MODTRAN in CAMEO-SIM) should in general be applied before the actual sensor model.

3.2 MultimIR

Basics	**Filter Transmission**	**Optics**	**Detector**
Fov: 5.3° x 4.0° 35° x 26° Optics: 15 mm F/2 or 100 mm F/2 Resolution: 384 x 288 Atmospherics: MODTRAN [4] MTF (Eq. (2.39) and Eq. (2.45)) Motion: MTF (Eq. (2.36) and Eq. (2.38))	Filter 1: 1.55-1.75 μm Filter 2: 2.05-2.45 μm Filter 3: 3.45-4.15 μm Filter 4: 4.55-5.2 μm	Transmission: $T(\lambda)$ MTF: Cascaded Gaussian	Pitch: 24 x 24 μm Pixel Size: 20 x 20 μm Fill Factor: 69 % Semiconductor: HgCdTe λ_{cutoff} = 5.2 μm $t_{Integration}$ = 2.6 ms Response: $R_{rel}(\lambda)$ Conversion: K Measured / Adjusted Dynamic Range: 14 bit (2^{14} levels) Basic Noise: Gaussian White Colour Mean μ_y (Eq. (2.25)) Variance σ_y^2 (Eq. (2.30)) MTF: Eq. (2.33)

Table 3.1. Variables and functions with some default values for a basic MultimIR sensor model.

The MultimIR [20,38-40] is a short- to midwave IR focal plane array (FPA) camera with two sets of optics. It has four wave band selection filters (which sits in front of the optics on a rotating wheel), a 384 x 288 HgCdTe semiconductor array, and a 14 bit output dynamic range. The

implementation should be made so that a ‘push on a button’ would give the user the possibility to degrade synthetic imagery according to an approximate MultimIR sensor model with default values. Naturally, these values should be possible to alter. The radiative signal passes through the spectral filter for wave band selection and is transmitted and smeared through the optics. It then reaches the detector array elements were the signal is converted through a spectral response to a voltage. This voltage is amplified and converted to a digital number via a conversion number. Noise is added through the chain described before it can be converted via calibration to a radiometric unit such as radiance or apparent temperature. Using the theoretical discussion in section 2, a basic sensor model for the MultimIR for synthetic imagery input should follow the functions and variables as outlined in table 3.1 with some default values indicated. Not mentioned here is the difficult, but fundamental fixed pattern noised that has to be included at least for MultimIR image reconstruction as well as dead pixel corrections.

3.3 Emerald

The Emerald [39,40] system is quite similar to the MultimIR and hence the values in table 3.1. There are a few differences. First of all the optics is a 50 mm F/2 telescope with a fov of 17° x 14°, and it has 640 x 512 pixels made out of InSb with a $\lambda_{cutoff}^{effective}$ = 5.1 μm. The system is furthermore equipped with three different filter transmission selections to obtain three optical wavebands, i.e. with band 1 < 3.9 μm, band 2 ≈ 3.3 – 5.1 μm, and band 3 > 4.6 μm. The pixels are 20 x 20 μm in size with a detector element pitch of 24 μm. The Emerald system can in many ways be treated in a similar manner as the MultimIR in section 3.2, also concerning noise.

3.4 QWIP

The QWIP [19] system is different from both the Emerald and the MultimIR in several ways. First of all the QWIP has its sensitivity in the longwave infrared (LWIR), and here the relative spectral response often is approximated with a Gaussian as shown in figure 3.2. The system at FOI has a QWIP sensor with 320 x 240 pixels, where each pixel is about 30 μm and where the pixel pitch is about 38 μm. The QWIP system is usually equipped with 20° x 15° fov telescope with a focal length of 40 mm and a f-number equal to 1. When it comes to noise considerations, dark current

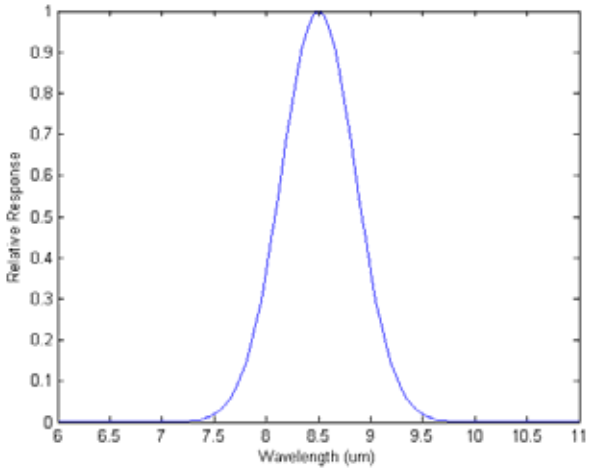

Figure 3.2. Approximate spectral relative response for QWIP [19].

gives the largest contribution and a Gaussian white noise model as suggested in section 2.2.2.1 is sufficient as a first approximation as the noise floor. The optical transmission can be considered to be ideal, i.e. 100% while the fill factor is around 62%.

3.5 Simple VIS-NIR CCD model

For completion, a simple model for a CCD Si based camera will be outlined. The fov is usually not given for commercial digital cameras, but rather the zoom, e.g. 28-105 mm, which means what focal lengths are available. If *f* is the focal length, then the fov is given by

$$fov = 2\tan^{-1}\left(\frac{l/2}{f}\right), \tag{3.1}$$

where *l* is the dimension of the detector. (E.g. 35 mm film means a 36 x 24 mm sized detector. Remember that it is more or less the size of the recording medium that decides the fov.) The aperture is also most likely not a fixed number and can hence be altered by the user. As before (assuming the object is at infinity), the f-number is given as the ratio between focal length and aperture diameter. A Si based CCD has an optical cutoff at about 1.1 μm, i.e. radiation with wavelengths longer than 1.1 μm is not collected. The number of pixels in a CCD detector, especially for a digital camera for commercial use can be quite high. In the FOI CCD sensor system Redlake [40,41], the number of pixels is 1392 x 1040 with a pixel size of 4.65 x 4.65 μm, and with a pixel pitch of 5.5 μm. The fill factor of such a system is then about 72%. The FOI Redlake system has 3 CCDs, where 3 different prisms with selective filters in the green, red and near-IR produces 3 simultaneous digital images in those wavebands [40,41]. The integration time as well as the aperture of the Redlake CCD system can be set manually [41] for different applications. Integration time can also be set to automatic for optimal signal strength. Spectral response of this system can be approximated with the product of the spectral response of the CCD (Si) and the selective filter.

For commercial CCD RGB cameras, the pixels are often sorted in the so called Bayer pattern [42],

R	G	R	G
G	B	G	B
R	G	R	G
G	B	G	B

Figure 3.3. Bayer pattern for an RGB CCD array.

as indicated in figure 3.3, where R stands for red, G for green, and B for blue. This means that 50% of the pixels are green, 25% red, and another 25% blue. By interpolating this Bayer pattern, three complete red, green and blue images are obtained, which then can be added together (in a suitable format) to produce a digital color image. Often the pixel has an 8 bit color depth (other color depths are also very common), i.e. each pixel can have any of $2^8 = 256$ luminance levels, where (255,255,255) is perfect white and (0,0,0) is perfect black. In practice, each pixel is covered with a color selective filter (often painted right on top of the semiconductor pixel), see e.g. [42]. Normally, commercial digital cameras can export to a number of standard image formats [42], e.g. JPEG. A synthetic RGB color image would then be constructed by simulating a scene from 0.38 to 0.78 μm with a unit spectral response, and with a bandwidth of say 10 nm. This spectral image can then be transferred through suitable MTFs corresponding to everything before the actual detector. Pixels are sorted as indicated in figure 3.3 using suitable spectral responses for blue, green and red. A complete image for each color is constructed, and finally the three color images are processed to form an RGB image with a certain color depth (dynamic range). Noise could be added more or less at any stage if only a Gaussian white noise model is satisfactory. It should also be noted that there exists pixel matrices for colour cameras were each pixel gives all three colours [42]. As a photon of different wavelength has different energies and therefore different mean penetration depths in the semiconductor material at hand, photons corresponding to red (longest wavelength)

can be separated from green and blue (shortest wavelengths) by redout from the pixel side [42]. In this case all pixels give all three colors and hence increase available color and radiance information [42].

There are also various different light amplifying sensors in the visual and near-IR domain for low light levels. The main type uses photomultiplier tubes for light amplification and much of the constituents of such a system can be treated using MTF describing contrast reducing physical phenomenon [25]. There are also new systems were the amplification is done within the pixel semiconductor structure [22].

3.6 MTF

It is important that the MTFs described in section 2 are implemented correctly. The findings of equation (2.4) and equation (2.8) may be used, i.e. the Fourier transform of the output is equal to the MTF multiplied with the Fourier transform of the input as

$$G(u,v) = F(u,v) \times H(u,v), \tag{3.2}$$

where *F(u,v)* is the input frequency spectrum using a so called discrete fourier transform (DFT), and *H(u,v)* is the total MTF of the sensor system. When multiplying on a point-by-point basis the MTF with the image spectrum, the MTF must have the same size as the image spectrum, i.e. the same number of pixels. This is done by sampling the MTF up to the Nyquist frequency, i.e. up to half the sampling frequency. This is illustrated in figure 3.4 below, where the Nyquist frequency location is indicated. If the MTF (*H(u,v)* is equation (3.2)) is sampled correctly with the dimensions of the input *f(x,y)*, the final result can be written as

$$g(x,y) = DFT^{-1}\big(G(u,v)\big) = DFT^{-1}\big\{DFT\big(f(x,y) \times MTF_{System}(u,v)\big\}. \tag{3.3}$$

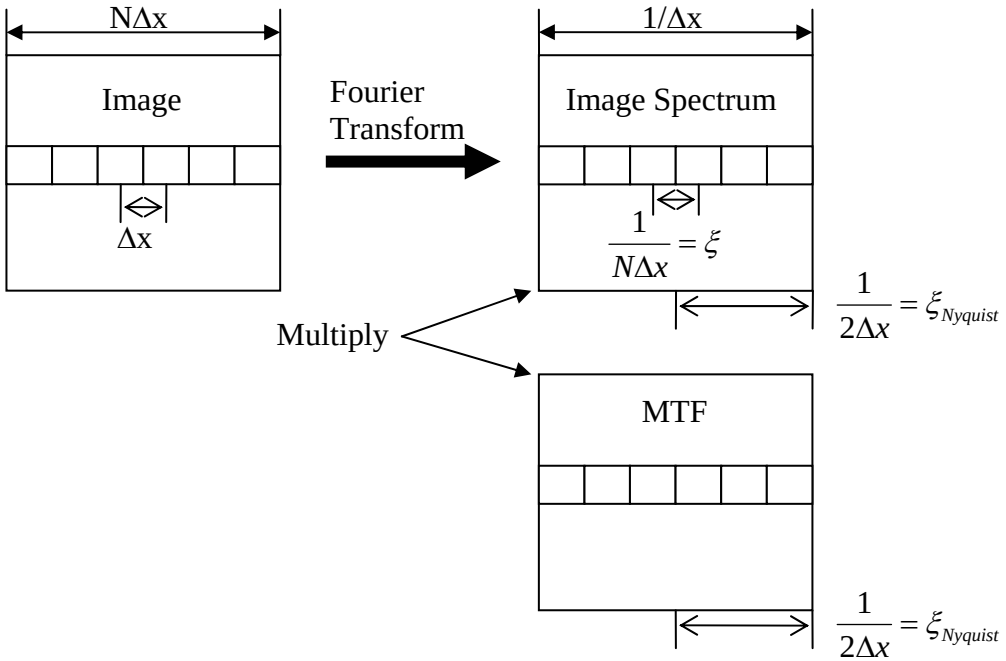

Figure 3.4. Nyquist location when using Discrete Fourier Transfrom [25].

As suggested in the work by Ientilucci [25], that the MTF should be sampled using the Nyquist criteria, the limit of frequency sampling in the MTF array will be set by the Nyquist criterion. This means that the MTF will consist of modulation values up to the Nyquist frequency. The frequency

cutoff is set by the smallest frequency cutoff of all the individual MTFs included in $MTF_{System}(u,v)$ in equation (3.3). E.g., if the sensor system only consist of an MTF given by

$$MTF_{System} = MTF_{Diffraction} \times MTF_{Detector}\,, \tag{3.4}$$

and the detector cutoff, f_{dco}, is smaller than the optical cutoff, f_{oco}, then MTF_{System} will consist of modulation values calculated up to $\frac{1}{2} f_{dco}$.

When using MTF as a sharpening filter, e.g. for image reconstruction, solve instead equation (3.3) for $f(x,y)$, i.e. if an experimental radiance map, $g(x,y)$ is obtained e.g. from an imager, the sharpened image $f(x,y)$ will be given by

$$f(x,y) = DFT^{-1}\left(\frac{DFT\big(g(x,y)\big)}{MTF\big(u,v\big)}\right). \tag{3.5}$$

As a division is carried out where small numbers might be involed, it might be necessary to stabilse the solution in equation (3.5). This can be done by implementing the so called Wiener-solution. Equation (3.5) can then be re-written as

$$f(x,y) = DFT^{-1}\left(\frac{MTF(u,v)}{MTF(u,v)^2 + \dfrac{N^*(u,v)N(u,v)}{DFT^*\big(g(x,y)\big)\times DFT\big(g(x,y)\big)}} \times DFT\big(g(x,y)\big)\right), \tag{3.6}$$

where $N(u,v)$ is the measuring noise from the fourier transform of $g(x,y)$, and where $N^*(u,v)$ is its complex conjugate. A good value for the measuring noise is to choose the mean of the noise from $DFT^*\big(g(x,y)\big)\times DFT\big(g(x,y)\big)$, where $g(x,y)$ is the measured intensity image.

3.7 Output

Output can for an optical sensor system be presented in several ways. In this work the focus is on imagery even if detection probabilities, detection ranges etc are also important and very much used outputs for evaluating military optical systems and in signature assessment, see e.g. the NVTHERM program package [43]. There are several ways to output imagery. It can be done radiometrically, i.e. in units of radiance or apparent temperatures, or in digital numbers on a greyscale (which in turn can be calibrated into radiometrical units), in standard imagery outputs such as tiff, jpeg, bitmaps, etc. As the input from synthetic generated scenes is in radiance units, i.e $Wm^{-2}sr^{-1}$, and a conversion to digital number takes place, a second conversion is necessary to deliver radiometrical units. Export to standard imagery formats is trivial, but it should be noted what the imagery is intended to be used for later on. Conversion to apparent temperature units is a little bit trickier, but can be obtained using an iterative technique. Assume that the imagery is converted/calibrated back to radiance, L_{Image}, after going through the sensor steps. For a target temperature T, the spectral radiance, L_λ, is given by

$$L_\lambda(T) = \frac{2ch}{\lambda^5\left(e^{\frac{hc}{kT\lambda}} - 1\right)}, \tag{3.7}$$

where c is the speed of light, h is Planck's constant, k is Bolztmann's constant, and λ is the wavelength. By multiplying equation (3.7) with the total spectral response, $R(\lambda)$, of the optical system, the radiance from the wavelength interval $[\lambda_1, \lambda_2]$ can be obtained by integration, i.e.

$$L(T) = \int_{\lambda_1}^{\lambda_2} L_\lambda(T) R(\lambda) d\lambda \,. \tag{3.8}$$

By letting the difference between the modelled radiance, L_{Image}, and the radiance in equation (3.8) go to zero by iteratively chosing a new temperature T, the apparent temperature in each pixel of the image can be obtained, i.e.

$$\Delta L = L_{\mathrm{Im}age} - L(T) \to 0 \,. \tag{3.9}$$

There are a number of ways of implementing equation (3.9), e.g. using any number of numerical recipes such as Newton-Raphson, but the fastest is probably to plot equation (3.8) for a number of temperatures and use interpolation to find a temperature, $T_{Apparent}$, good enough to satisfy equation (3.9). The temperature, $T_{Apparent}$, will then be the apparent temperature of the pixel.

4. Examples

A Matlab example of how a sensor model can be constructed has been carried out. The first part consists of a simple routine of reading a raw hyperspectral CAMEO-SIM image. In the second part, sensor properties such as f-number, fov, detector size and pitch etc are defined. A third part carry out a calculation for gain estimation, e.g. for a thermal sensor a 300 K body should lie about in the middle of the sensor's dynamic range and for a visual camera a 6000 K body can be used in analogy. The next subroutine calculates all the MTFs involved and then the cascaded MTF is applied (differentially) on the hyperspectral image including an optical transmission factor. A poisson noise model for photon noise is applied differentially on the hyperspectral image and then the integrated image is formed by summing the differentials together. Another poisson model for the quantum conversion to electrons is added. The image is now ready for extra noise factors such as temporal and spatial noise as well as dead pixel simulation.

The first example shows a basic model describing the FOI system MultimIR, and a second example shows a model on how three different bands are extracted from a hyperspectral simulation to be combined into a 10-bit RGB image.

4.1 MultimIR

In this section, a simplified model of the FOI system MultimIR [20] has been constructed to illustrate how a sensor model (at least in principle) can be implemented. The MultimIR as 4 filter bands of interest, ranging from 1.55 μm to 5.2 μm. In this illustration a synthetic image has been generated using the CAMEO-SIM [1] tool to simulate the MultimIR filter 4 thermal band. The transmission curve of this filter has not been used directly in CAMEO-SIM. Instead a hyperspectral simulation has been carried out to cover the filter 4 thermal band using a unity transmission curve between 4.0 and 5.12 μm. This hyperspectral image has been processed through steps modelling the filter transmission, the MultimIR 100 mm optics, and implementing a Gaussian white noise model for estimating temporal noise. A conversion gain has been estimated by letting a 300 blackbody correspond to the middle of the MultimIR 14 bit dynamic range transmitted through 1900 m of vertical atmosphere calculated by MODTRAN [4]. A downward facing sensor has been simulated to be onboard a plane travelling at 166 km/h at 1900 m above ground with small random vibrations corresponding to a detector angular subtense of 25 %. A total MTF describing diffraction, average optical aberrations (the semiempircal formula for well-designed optics in equation (2.12)), detector, linear and random motion has been implemented following the implementation discussion in section 3. The implementation has been done in Matlab using the "Image Processing Toolbox". Figure 4.1 shows the resulting synthetic image simulating the MultimIR with 100 mm optics and the thermal transmission filter 4 band together with the applied total MTF. A 0.5% dead pixel rate (so called 'salt and pepper' noise) has been added as well. The sensor is travelling from left to right in figure 4.1.

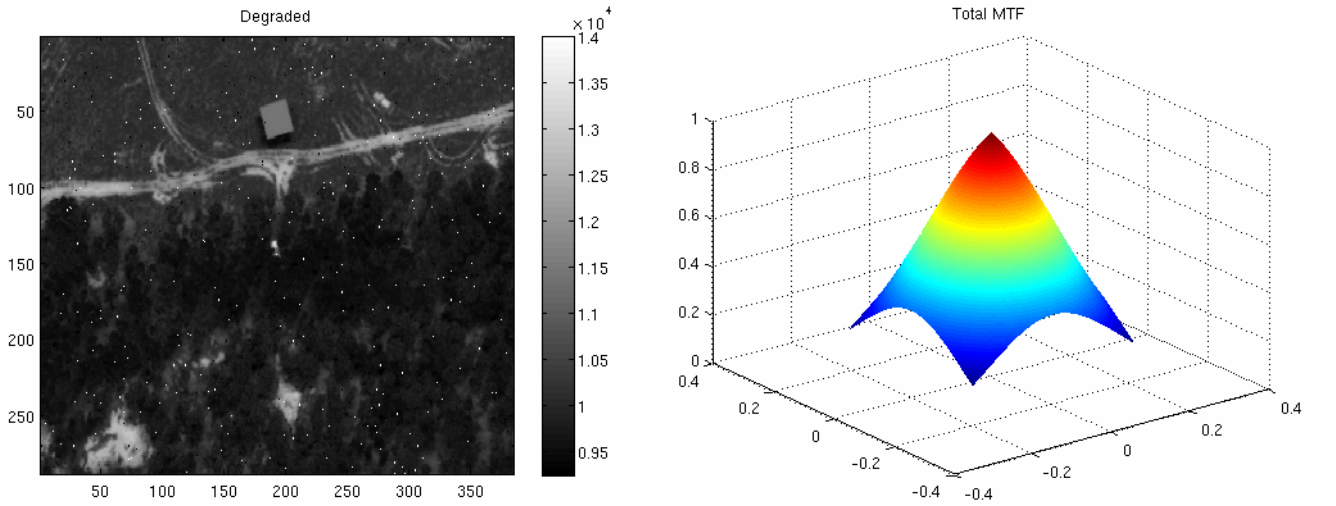

Figure 4.1. Simulated synthetic image of the FOI system MultimIR [20] equipped with 100 mm optics and filter 4 (thermal waveband) to the left. Total applied MTF including optics, movement, and detector averaging to the right.

Inspecting figure 4.1 it can be seen that no fixed pattern noise (except simulated dead pixels) is included in the simulation. The temporal noise is based upon measurements carried out as described in section 2.2.2.1 [44]. In this way, values for temporal noise (equation (2.47)) and dark current (equation (2.36)), has been included in the sensor model according to section 2.2.2.1. As discussed in section 2.2.2.1, spatial noise (nonuniformity) is often the main limiting factor for thermal IR sensors [22]. The spatially correlated noise (e.g. bias but also gain) is not well behaved and dependent on such difficult variables such as sensor operating conditions. This makes the prediction of such noise effects difficult and from a synthetic imagery point of view nearly impossible to predict without sensor characterisation. However, nonuniformity can be corrected for as shown in figure 4.2. Figure 4.2 shows real MultimIR imagery without correction (left) and with correction right. In this way, the need for modelling nonuniformity from a total synthetic

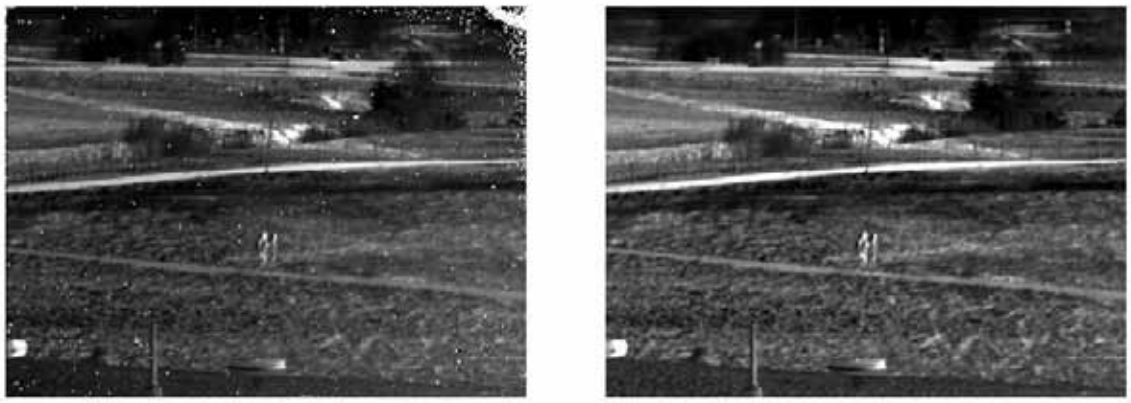

Figure 4.2. Real MultimIR imagery with uncorrected nonuniformities (left), and corrected uniformity (right) using filter 4.

imagery point of view might not be necessary. This should not be confused with the importance of modelling nonuniformity for image correction [40,44,45], so called nonuniformity correction (NUC). If on the other hand, a simulation of more raw imagery of an existing sensor is of interest, measured nonuniformity can be included in the image. Using nonuniformity measurements [40,44,45] the relationship [45]

$$\Delta Y_{jk} = Y_{jk} - \langle Y_k \rangle , \tag{4.1}$$

where Y_{jk} denotes the digital number for reference temperature [44,45] k for pixel j, and where $\langle Y_k \rangle$ is the mean digital number of the FPA for reference temperature k. By performing a least square polynomial fitting, the difference can be expressed as an approximation as [44,45]

$$\Delta Y_{jk} = Y_{jk} - \langle Y_k \rangle \approx \sum_{i=0}^{N} C_{ij} Y_j^i \,, \tag{4.2}$$

where C_{ij} are the fitted coefficients for pixel j and with a polynomial approximation of degree N. In this way a corrected signal can be expressed as

$$Y_j^c = Y_j - \sum_{i=0}^{N} C_{ij} Y_j^i \tag{4.3}$$

can be used, where Y_j is the digital number of pixel j, i = 0,1, and where C_{ij} are the least square

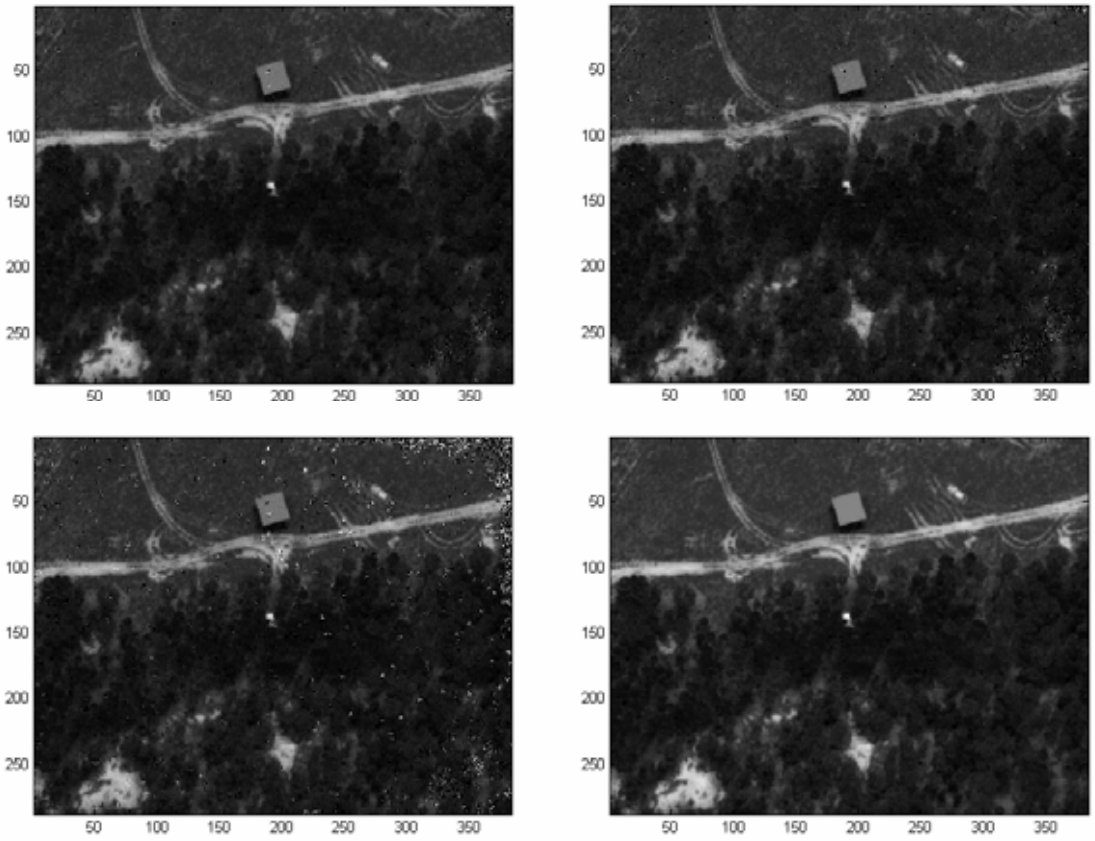

Figure 4.3. Measured spatial noise added to synthetic imagery at 3 different times. Lower right image shows the synthetic image without the added noise.

fitted coefficients. By calculating the standard deviation from a measured variation bias (see section 2.2.2.1) image as in equation (4.1) using a filter to get the standard deviation of each pixel from its 3 x 3 nearest neighbours and repeating that for the gain variation coefficient the total correlated spatial variation in equation (2.43) can be calculated. In figure 4.3, three different nonuniformity measurements have been carried out [44] and added to the synthetic image in figure 4.1. Dead pixels has not been added using a “salt and pepper” scheme as in figure 4.1. Inspecting the three images where noise has been added according to equation (4.3), the images not only shows large differences from the original synthetic image (lower right corner of figure 4.3), but also amongst each other. Note also the noise similarities between left image in figure 4.2 and the simulated bottom left corner image in figure 4.3. The differences between these three noisemeasurements are only the time at which they were taken. Please note that the dynamic range

of the scene is quite small, and that maximum and minimum digital number range has not been optimised for best image.

4.2 Three band sensor model

In this example a synthetic hyperspectral image has been simulated using the same scene as in the previous example (see section 4.1). The wavelength interval was 450 – 880 nm with a resolution of 5 nm. A sensor matrix consisting of 696 x 520 pixels were used with pixel sizes and pixel

B G R

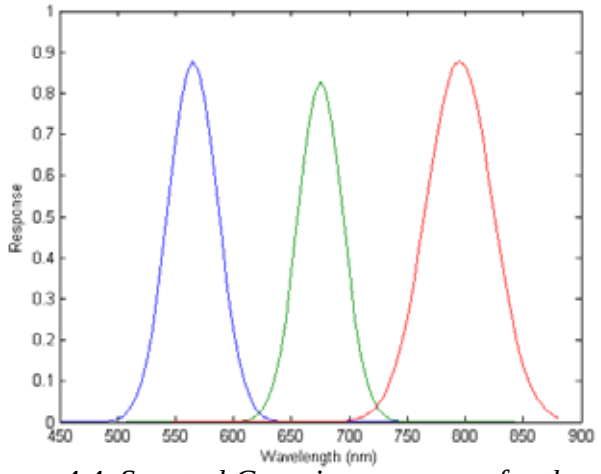

Figure 4.4. Spectral Gaussian responses for three band selections.

pitches of 4.65 and 5.5 μm, respectively. The fov corresponded to a focal length of 28 mm. An f-number of 11 was used. The synthetic hypersectral image was simulated with unit response in the wavelength interval. In the model three spectral responsive bands were given in form of three Gaussians as shown in figure 4.4. The corresponding three radiance images from the spectral responses in figure 4.4 were calculated using a total conversion gain simulating a 10 bit sensor, i.e.

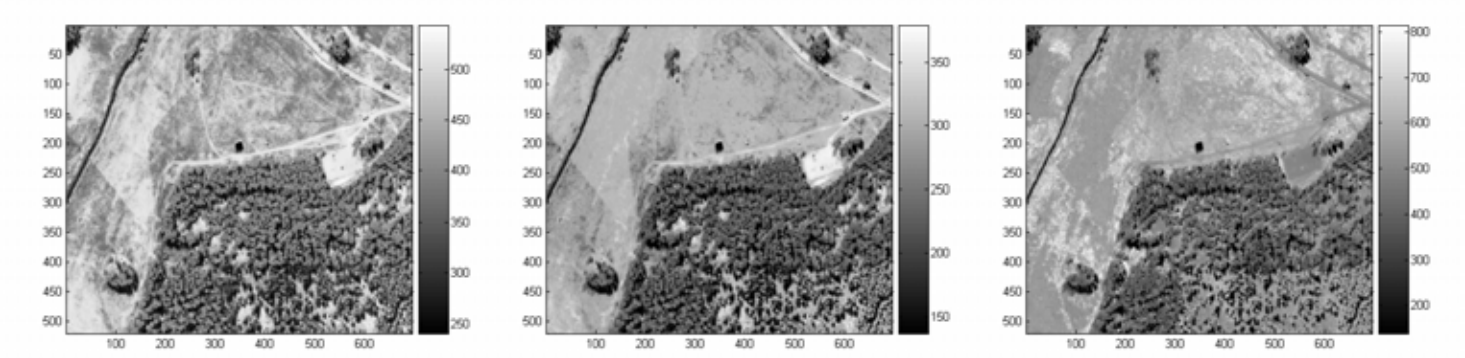

Figure 4.5. Three synthetic images (in digital numbers) corresponding to the three Gaussian responses in figure 4.5 from left to right.

2^{10} levels. The conversion gain was defined as giving half the full dynamic level of the sensor for the mean value in the near-infrared (NIR) response in figure 4.4 (red curve). In figure 4.5 the three images for the three responses in figure 4.4 are shown going in increasing wavelength from left to right. By letting the shortest wavelength band correspond to blue, the midband to green, and the NIR to red an RGB image (as indicated at the top of figure 4.4) could be constructed showing e.g. the grass reflectance as blue color and the NIR reflectance as red.

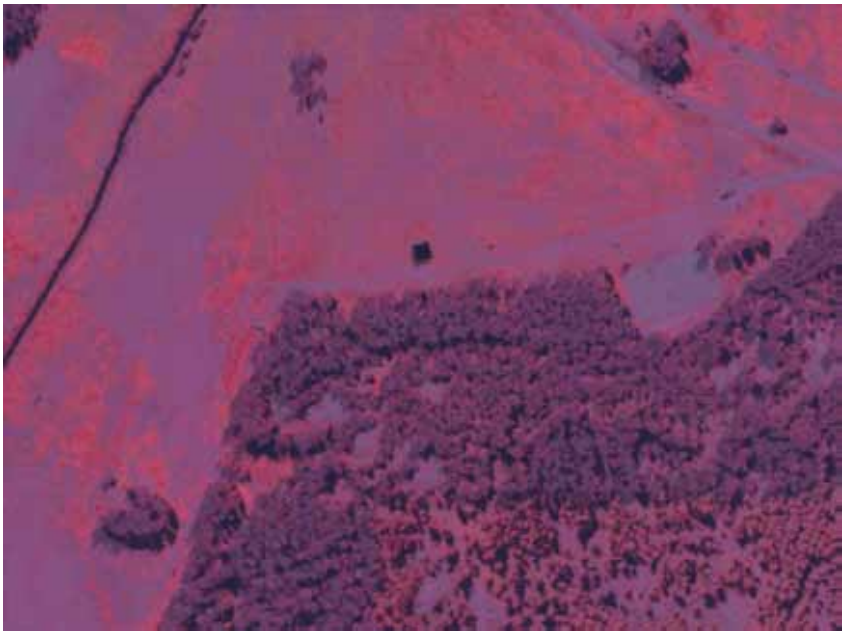

Figure 4.6. RGB image where colors corresponds to the spectral responses in figure 4.5.

5. Final remarks

In this work, a sensormodel has been created aiming at as accurately as possible complement available synthetic imagery generating tools in the optical wavelength domain. Basic sets of formulas for image degradation has been outlined, including sensor effects such as optical degradation, finite pixel resolution, noise, but also effects that are common for operating sensor systems such as motion, vibrations, and atmospheric turbulence. A discussion on implementation is also given as well as a few introductory examples showing typical results. The next step is to develop software in which a sensor model as outlined in this work is implemented. This software should not only cover synthetic imagery generation, but should also include sensor system characterisation possibilities.

References

[1] Insys Ltd, *User Manuals, CAMEO-SIM v. 5.5.1*, 2006.
[2] www.thermoanalytics.com
[3] Insys Ltd, User Manuals, *McCavity v 4.0*, 2005.
[4] F.X. Kneizy et al., *The MODTRAN 2/3 Report and LOWTRAN 7 Model*, Phillips Laboratory, Geophysics Directorate, PL/GPOS Hanscom AFB MA 01731-3010, USA, 1996.
[5] G. Boreman, *Infrared Systems Design*, lecture notes, FOI, Linköping, 2004.
[6] G. Boreman, *MTF in Optical & Electro-Optical Systems*, lecture notes, FOI, Linköping, 2002.
[7] E. Hecht, "Optics", Addison-Wesley, ISBN 0-201-11611-1, 1987.
[8] G.C. Holst, "Electro-Optical Imaging System Performance", SPIE Optical Engineering Press, Winter Park, Florida 32789, 1995.
[9] J.W. Goodman, *Introduction to Fourier Optics*, 2nd ed, McGraw-Hill, 1996.
[10] *R.R. Shannon, Aberrations and their effects on images*, SPIE Proceedings Vol. 531, p- 27, 1985.
[11] M. Born and E. Wolf, *Principles of Optics*, 3rd edition, pp 468-469, Pergamon Press, NewYork, 1965.
[12] G.C. Holst, *Electro-Optical Imaging System Performance*, p. 106, SPIE Optical Engineering Press, Winter Park, Florida 32789, 1995.
[13] L. Levi and R. Austing, *Tables of the MTF of a Defocussed Perfect Lens*, Applied Optics, Vol. 7(5), pp. 967-974, 1968 and Errata, Applied Optics, Vol 7(11), p. 2258. 1968.
[14] R.R. Shannon, *A Useful Optical Engineering Approximation*, Optics & Photonics, p. 34, 1994.
[15] G.C. Holst, *Electro-Optical Imaging System Performance*, pp. 104-105, SPIE Optical Engineering Press, Winter Park, Florida 32789, 1995.
[16] G.H. Rieke, *Detection of light from the Ultraviolett to the submillimeter*, Cambridge University Press, New York, 1994.
[17] S.M. Sze, *Semiconducotor Devices, physics and technology*, John Wiley & Sons, New York, 1985.
[18] S.B. Campana, *The Infrared & Electro-Optical Systems Handbook, Volume 5, Passive Electro-Optical Systems*, pp. 160-163, SPIE Optical Engineering Press, Bellingham, Washington, 1993.
[19] www.acreo.se/templates/Page____996.aspx
[20] I. Renhorn et al., *Försök med multispektrala aktiva/passive sensorer*, FOI-R--0290--SE, 2001.
[21] F. Dierks, *Sensitivity and Image Quality of Digital Cameras*, www.baslerweb.com, 2004.
[22] I. Renhorn et al., *TBD*, FOI-R--xxxx--SE, 2006.
[23] Equation 3 in *FLIR92 Thermal Imaging Systems Performance Model, Analyst's Reference Guide*, Document RG5008993, Ft. Belvoir, VA, 1993.
[24] C. Wigren, "IGOSS – Model of Image Generation in Optronic Sensor Systems", FOA-R--97-00582-616--SE, 1997.
[25] E. J. Ientilucci, "Synthetic Simulation and Modeling of Image Intensified CCDs (IICCD), Master Thesis, Center for Imaging Science in the College of Science, Rochester Institute of Technology, 2000.
[26] Equation 7 in *FLIR92 Thermal Imaging Systems Performance Model, Analyst's Reference Guide*, Document RG5008993, Ft. Belvoir, VA, 1993.
[27] *FLIR92 Thermal Imaging Systems Performance Model, Analyst's Reference Guide*, Document RG5008993, Ft. Belvoir, VA, 1993.

[28] Equation 8 in *FLIR92 Thermal Imaging Systems Performance Model, Analyst's Reference Guide,* Document RG5008993, Ft. Belvoir, VA, 1993.
[29] G.C. Holst, *Electro-Optical Imaging System Performance*, pp. 116-117, SPIE Optical Engineering Press, Winter Park, Florida 32789, 1995.
[30] G.C. Holst, *Electro-Optical Imaging System Performance*, pp. 313-323, SPIE Optical Engineering Press, Winter Park, Florida 32789, 1995.
[31] D.L. Fried, *Optical Resolution Through a Randomly Inhomogenous Medium for Very Long and Very Short Exposures*, Journal of the Optical Society of America, Vol. 56(10), pp. 1372-1379, 1966.
[32] D.L. Fried, Limiting *Resolution Looking Down Through the Atmosphere*, Journal of the Optical Society of America, Vol. 56(10), pp. 1380-1384, 1966.
[33] See e.g., J.W. Goodman, *Statistical Optics*, pp. 402-433, Wiley-Interscience, New York, 1985.
[34] F. Lei and H.J. Tiziani, *Atmospheric Influence on Image Quality of Airborne Photographs,* Optical Engineering, Vol. 32(9), pp. 2271-2280, 1993.
[35] I. Renhorn, *Inverkan av atmosfärsturbulens vid småmålsdetektion*, FOI-R--0715--SE, 2002.
[36] N.S. Kopeika, *Spatial-frequency and Wavelength Dependence Effects of Aerosols on The Atmospheric Modulation Transfer Function,* Journal of the Optical Society of America, Vol. 72(8), pp. 1092-1094, 1982.
[37] T. Kaurila et al., *Aerosol extinction models based on two measurements at two sites in Sweden,* Applied Optics, Vol. 45(26), p. 6750, 2006.
[38] L. Klasén et al., *Optroniska sensorsystem för ökad spaningsförmåga*, FOI-R--1104--SE, 2003.
[39] T. Chevalier et al., *Optroniska system 2004*, FOI-R--1422--SE, 2004.
[40] J. Ahlberg et al., *Multispektrala IR- & EO-sensorer,* FOI-R--1815--SE, 2005.
[41] See e.g., www.redlake.com
[42] See e.g., R.F. Lyon, *A Brief History of 'Pixel'*, Reprint-Paper EI 6069-1, Digital Photography II – Invited Paper, IS&T/SPIE Symposium on Electronic Imaging 15-19 January 2006, San Jose, California, USA.
[43] User's Manual & Reference Guide, *Night Vision Thermal Imaging Systems Performance Model,* U.S. Army Night Vision and Electronic Sensors Directorate, ATTN: AMSEL-RD-NV-MS-SPMD, Ft. Belvoir, VA 22060-5677, USA, 2001.
[44] W.Isoz, et al., *Nonuniformity correction of infrared focal plane arrays*, Proc. SPIE, 5783, 949-960, 2005.
[45] W. Isoz, *Calibration of multispectral sensors,* Examensarbete, LiTH-ISY-EX-3651-2005, Linköpings Universitet, 2005.